

# **Confinement size determines the architecture of Ran-induced microtubule networks**

Ya Gai<sup>1</sup>, Brian Cook<sup>2</sup>, Sagar Setru<sup>3</sup>, Howard A. Stone<sup>1, \*</sup>, and Sabine Petry<sup>2, \*</sup>

<sup>1</sup>Department of Mechanical and Aerospace Engineering, Princeton University

<sup>2</sup>Department of Molecular Biology, Princeton University

<sup>3</sup>Lewis-Sigler Institute of Integrative Genomics, Princeton University

\*Correspondence to [hastone@princeton.edu](mailto:hastone@princeton.edu) and [spetry@princeton.edu](mailto:spetry@princeton.edu)

## **Supplementary Information**

## Note S1 Geometrical parameters of the microchannels and applied flow rates

We characterized the droplet size by  $D$ , the nominal diameter of a droplet when it is spherical. Since  $D$  is always larger than the microchannel depth  $H$ , the droplet remained in a disc shape inside the microchannel (Fig. 1d). Prior works studied the deformation of a droplet confined between two parallel plates in detail. These works suggest that  $D$  and  $D'$ , the droplet diameter at its midplane, follow Eq. S1.

$$\left(\frac{D}{H}\right)^2 \left( q + \frac{\pi}{4} \sqrt{2q} + 1 - \frac{3\pi^2}{32} \right) = \frac{D'}{D}$$
$$\text{where } q = \frac{1}{3} \left(\frac{H}{D}\right)^3 - \frac{1}{3} + \frac{\pi^2}{32} \quad \text{Eq. (S1)}$$

We measured  $D'$  from confocal images and then used Eq. S1 to convert  $D'$  into  $D$ .

**Table S1. Summary of the flow rates, microchannel geometrical parameters, and droplet sizes.**

**$Q_d$  and  $Q_c$  denote the disperse and continuous phase flow rates, respectively.**

$D$ ( $\mu m$ )	$W$ ( $\mu m$ )	$H$ ( $\mu m$ )	$Q_d$ (mL/hr)	$Q_c$ (mL/hr)
20	20	15	0.3	1
60	40	50	0.3	0.3
110	90	90	0.3	0.4

## Note S2 Radon Transform

This section describes how we generated the Radon Transform plots (Fig. 4f) from the raw images.

We broke down the workflow into three steps.

- Step 1 – Noise and background removal

To suppress noises and remove backgrounds, we inputted the raw images into ImageJ and used the embedded “Subtract Background” function. The function applies a legacy “rolling-ball” algorithm to correct and identify the background. The rolling ball radius (on a pixel basis) was manually set to exceed the sizes of core structures to our interests (i.e., clusters and asters) to ensure the correct denoise and background removal process.

- Step 2 – Segmentation

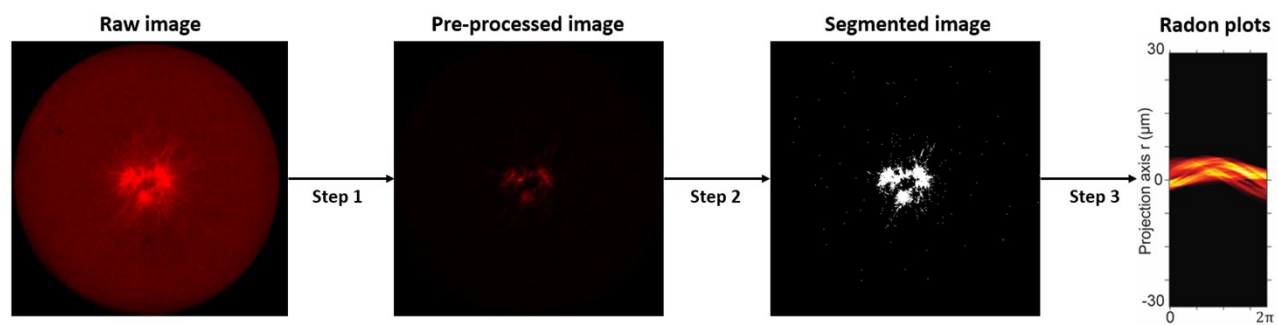
To segment the core structures required for Radon transform, we adopted the standard image segmentation pipeline in ImageJ. In short, we used the “*auto-threshold*” package to identify the brighter core structures characterized based on image intensity distributions. We proceeded to create image masks and transfer the segmented core structures onto the masks. The outputs from this step are ready for the Radon transform analysis.

- Step 3 – Radon transform

We fed the segmented images from Step 2 into MATLAB and used the “radon” function to generate the plots.

## Note S2 Figure

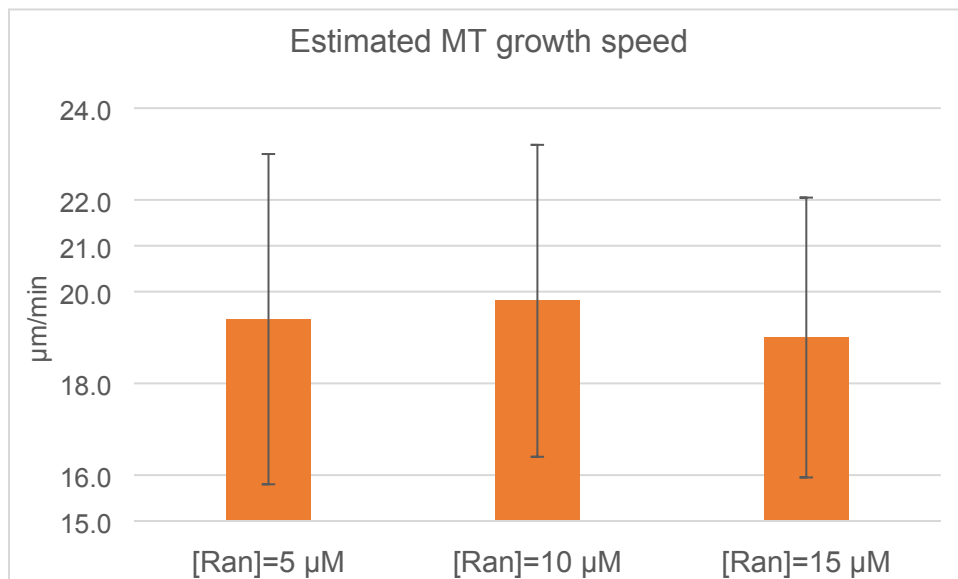
Illustration of the workflow for generating Radon transform plots. The raw image in this example corresponds to  $[Ran] = 10 \mu M$ ,  $D=60 \mu m$ , and  $t = 14 \text{ min}$ .



### Note S3 MT growth speed

Similar to the method for counting EB1 spots described in the main manuscript, we used the ImageJ TrackMate package for selecting and tracking EB1 spots to obtain MT growth speeds. The sample size, which refers to the total number of EB1 spots at a given condition of Ran concentration and droplet size, was limited mainly due to MT ends moving out of the focal plane and long exposure time between frames to ensure acceptable image qualities. The droplet size for all tests was 60  $\mu\text{m}$ . The measured results are summarized in the table and chart below. The error bar represents one standard deviation.

Ran concentration ( $\mu\text{M}$ )	5	10	20
Sample size N	10	9	9
Mean velocities ( $\mu\text{m}/\text{min}$ )	19.4	19.8	19.0
Standard deviation	7.2	6.8	6.1



### Note S3 Figure

An example of a selected EB1 particle used to estimate MT growth velocity. The particle is highlighted by the circle. The time in between two consecutive frames is 1.1 seconds.

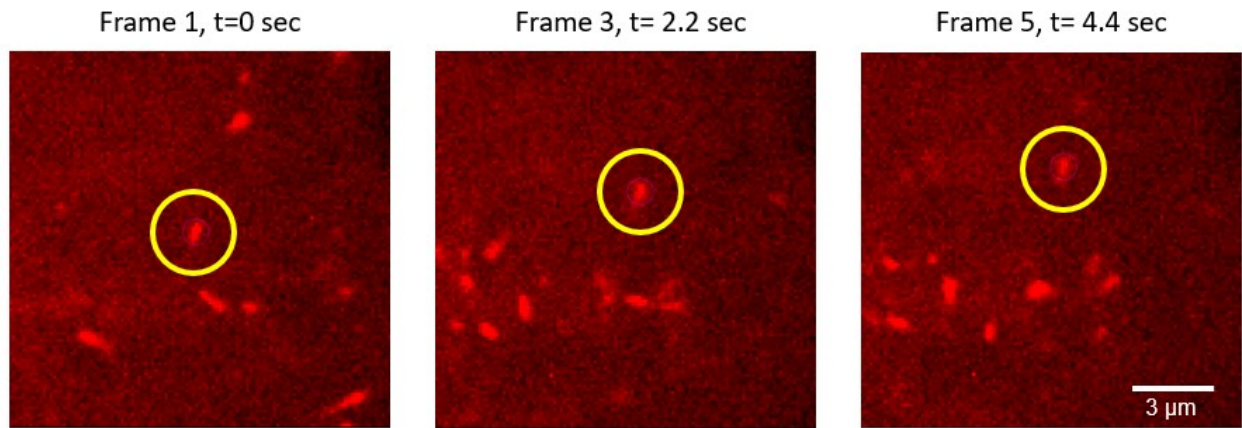
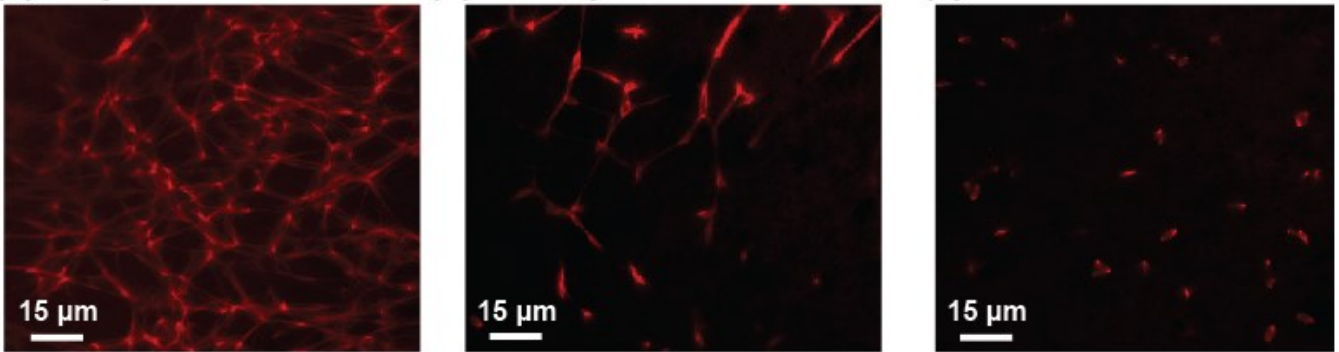


Figure S1. Ran-induced MT networks in bulk extracts at  $t=40 \text{ min}$

(a) Fully connected network (b) Partially connected network (c) Isolated mini structures



(d) Frequency of occurrence

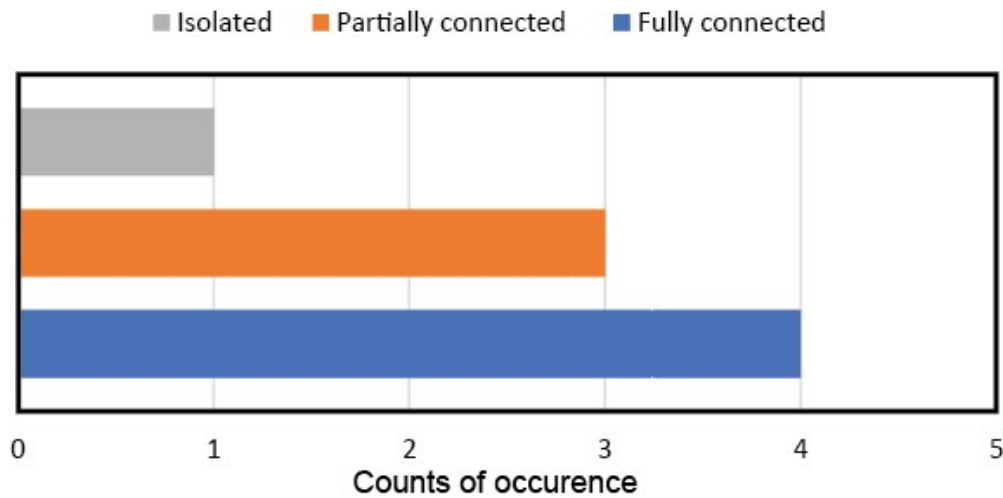
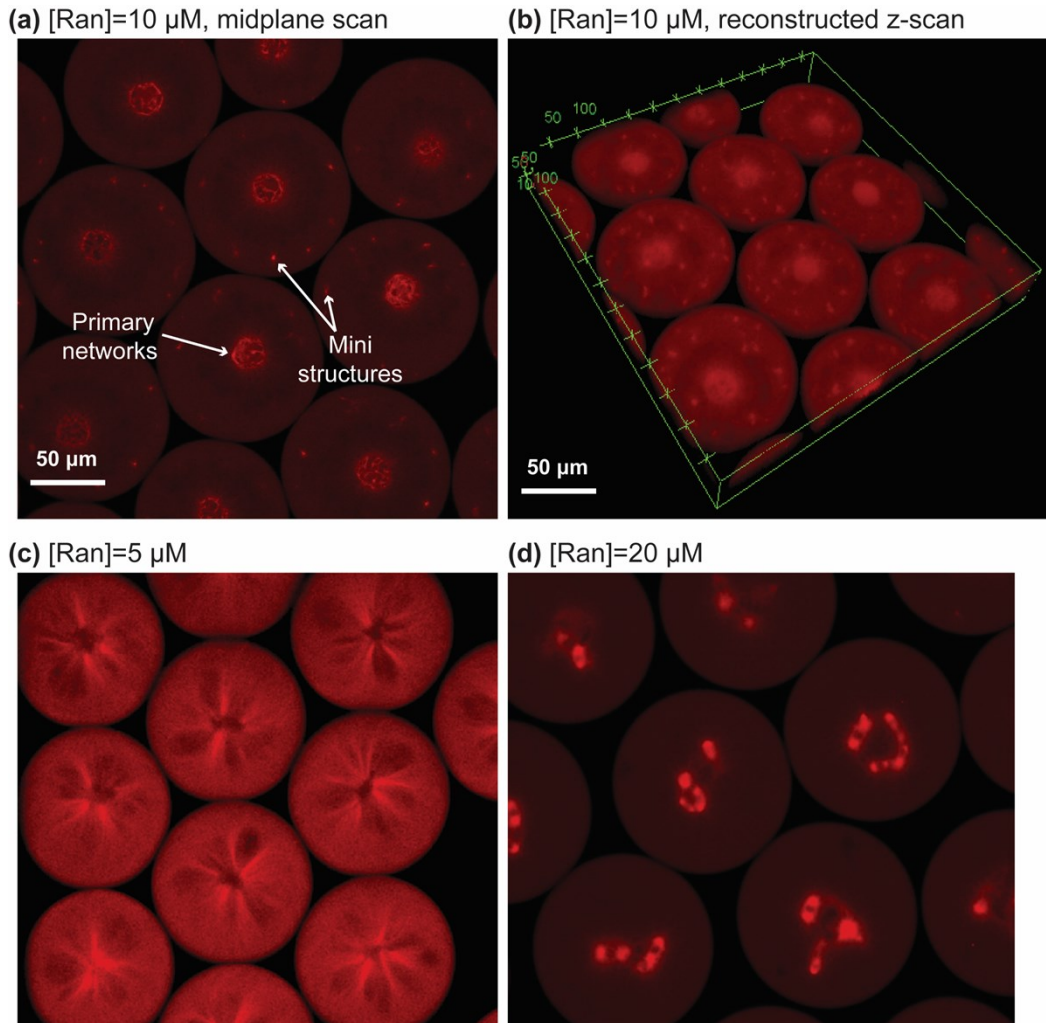


Figure S1. 3D projection of z-scan confocal images taken at  $t=40 \text{ min}$  for unconfined extracts. The Ran concentration is  $[Ran]=10 \mu\text{M}$ . Within the field of view, three types of MT network architectures were observed: (a) a fully connected network, where the MTs assembled into dense poles interconnected by thick MT bundles; (b) a partially connected network, where isolated structures and interconnected networks coexisted; (c) isolated mini structures only. (d) shows the frequency of occurrence from eight experiments, each corresponding to one extract preparation. Most of our experiments showed either fully or partially connected networks.

**Figure S2. Ran-induced MT networks in droplets at  $t=40 \text{ min}$**



Confocal images showing encapsulated extracts at  $t=40 \text{ min}$ . The size of all droplets is  $D=110 \mu\text{m}$ . (a)-(b) The ran concentration is  $[Ran]=10 \mu\text{M}$ . (a) Midplane image. (b) Reconstructed 3D image from z-direction scans. (c)  $[Ran]=5 \mu\text{M}$ . The flower-like structures remained unchanged at  $t=40 \text{ min}$ . (d)  $[Ran]=20 \mu\text{M}$ . At  $t=40 \text{ min}$ , the MT networks remained in multi-aster arrays inside each droplet, in contrast to the single asters shown in (a) and (b).

Figure S3. Wide-field images showing the assembly of MT rings

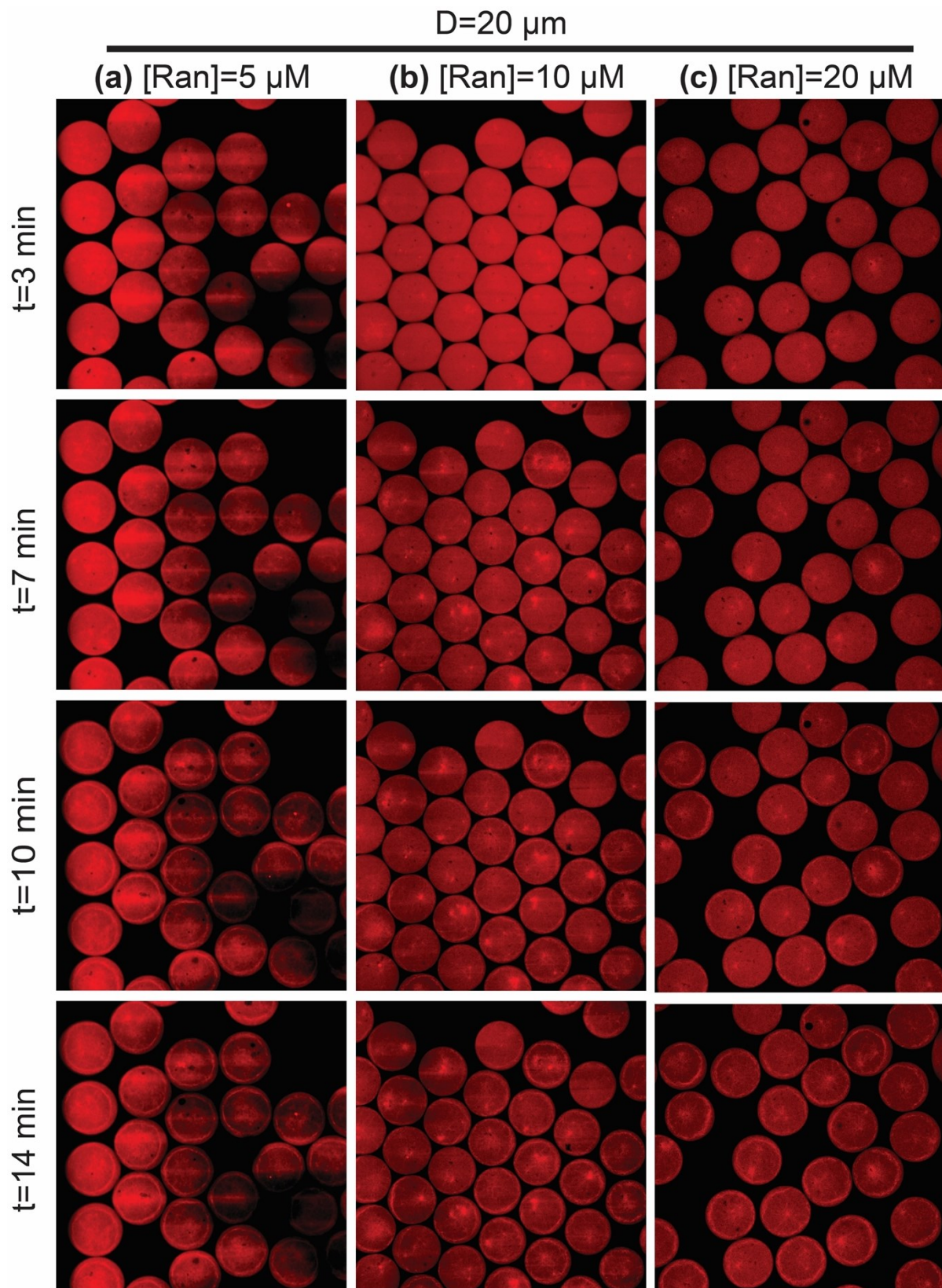
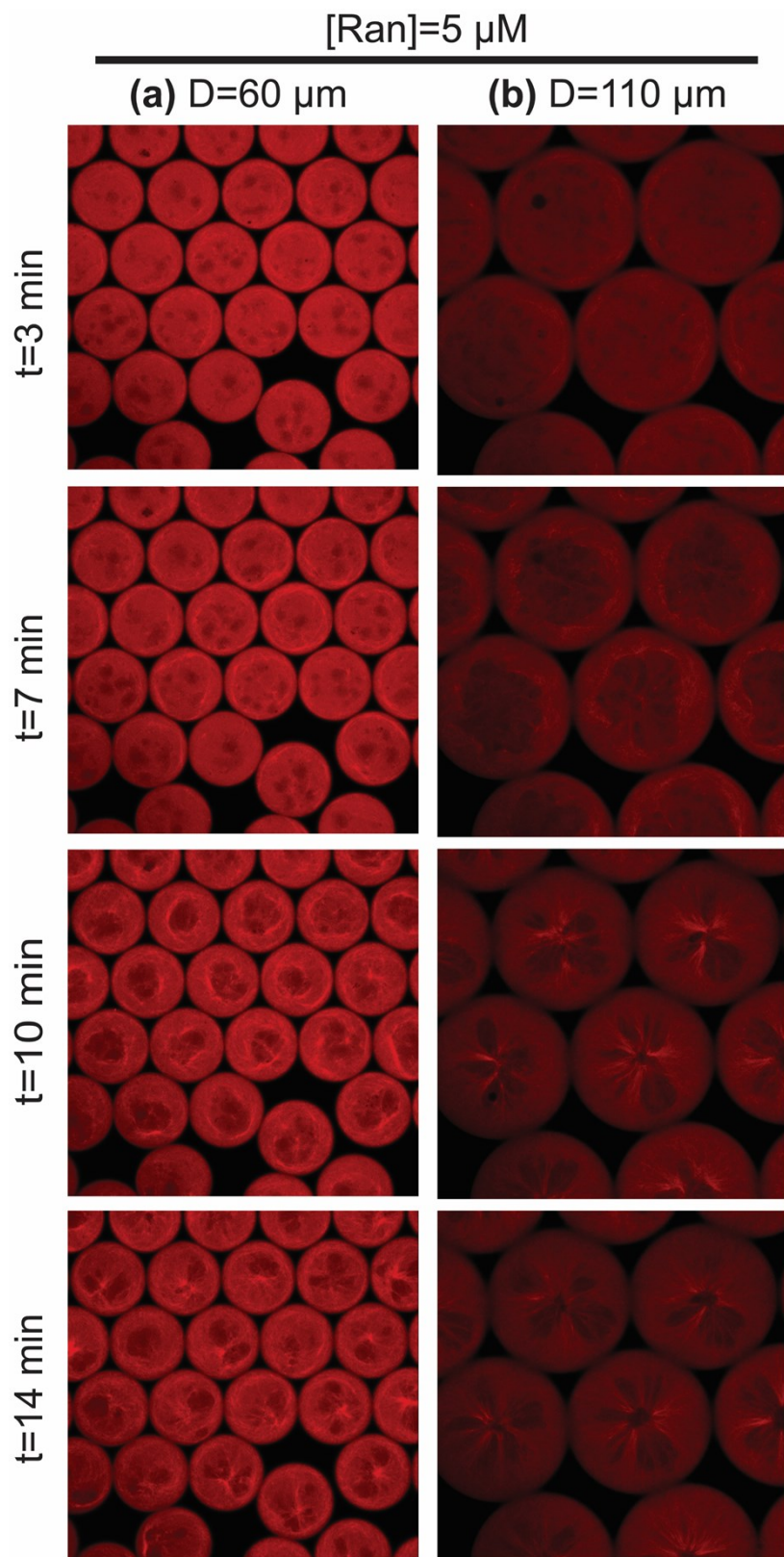
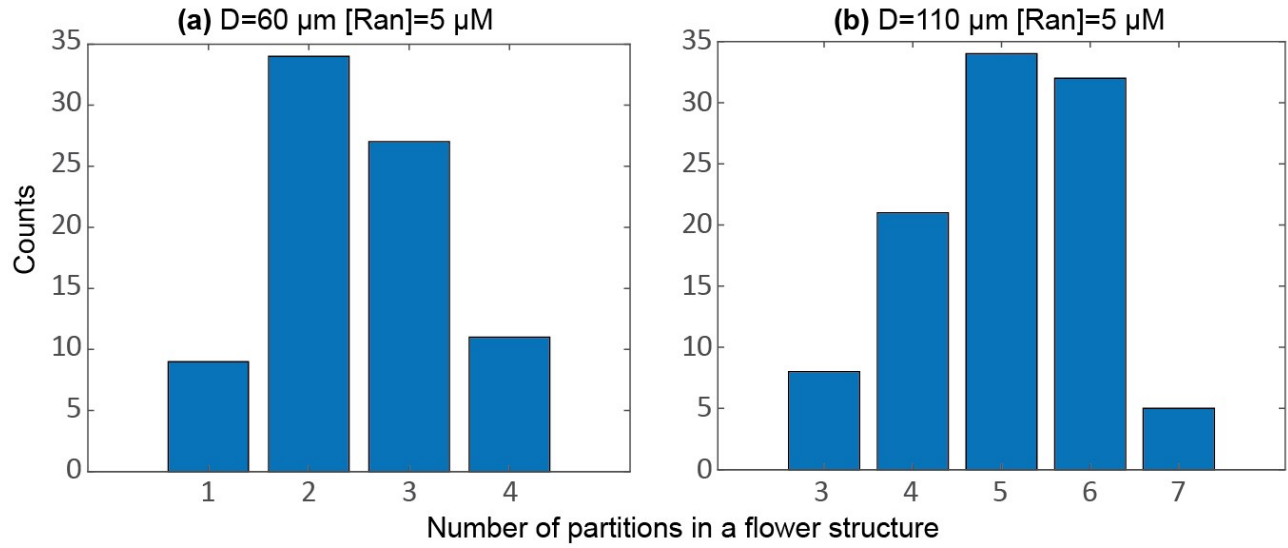


Figure S4. Wide-field images showing the assembly of flower structures



**Figure S5. Number of partitions in flower-shaped MT networks**



Number of partitions or void areas in flower-shaped MT networks. (a) The droplet size is  $D=60 \mu\text{m}$ . The histogram was generated by tracking a total of  $n=80$  droplets. The flower structure corresponds to Fig. 3(a) in the main text. (b) The droplet size is  $D=110 \mu\text{m}$ . The histogram was generated by tracking a total of  $n=80$  droplets. The flower structure corresponds to Fig. 3(b) in the main text.

**Figure S6. Effect of Taxol on the flower assembly**

The droplet diameter is  $D=110 \mu\text{m}$ . The Ran concentration is  $[Ran]=5 \mu\text{M}$ . The final concentration of Taxol was set at  $40 \mu\text{M}$ .

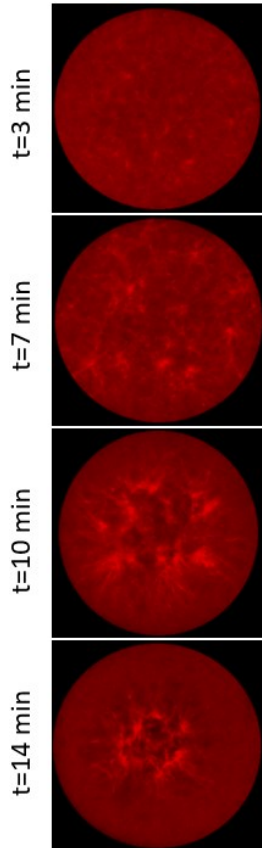
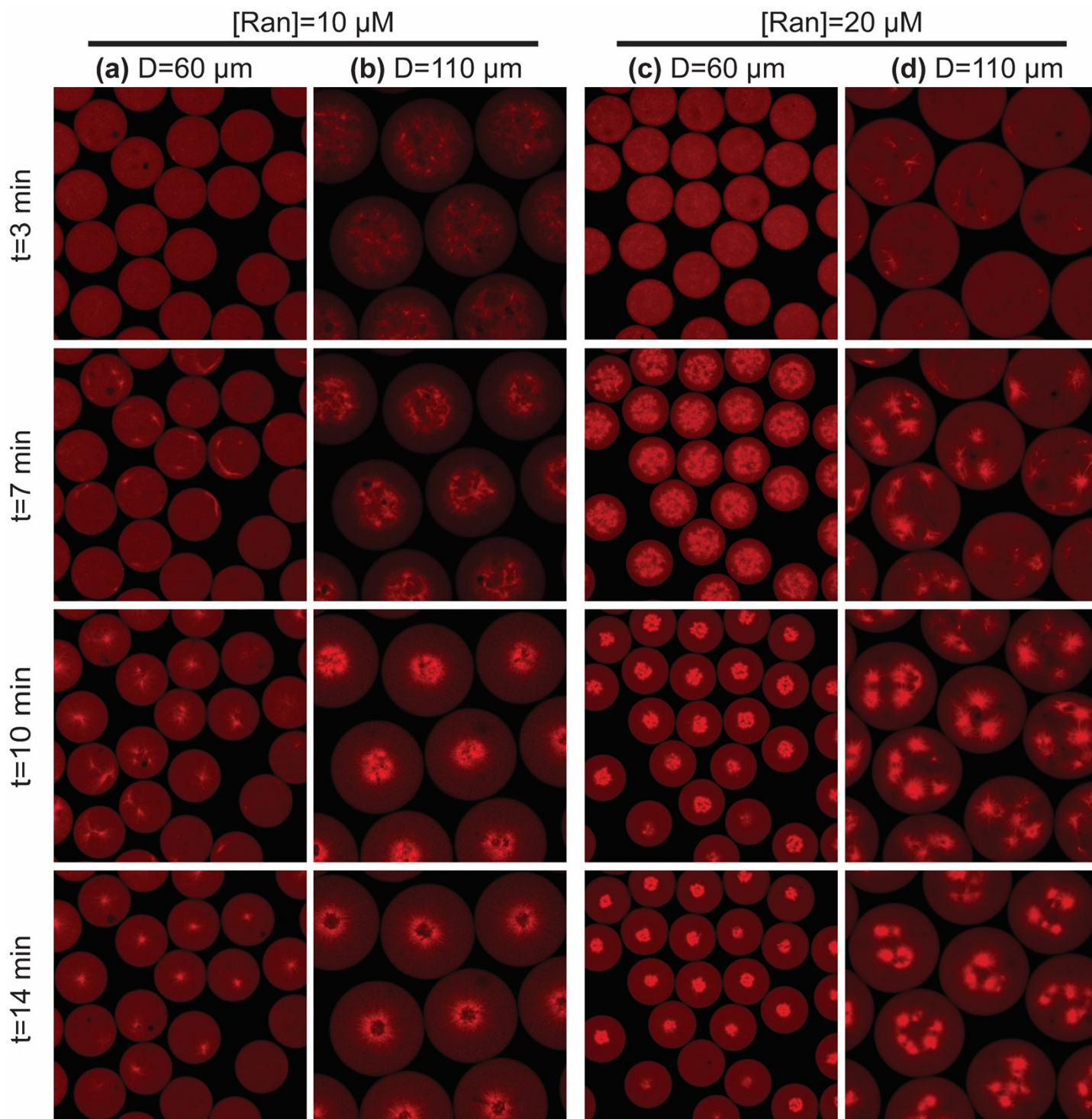
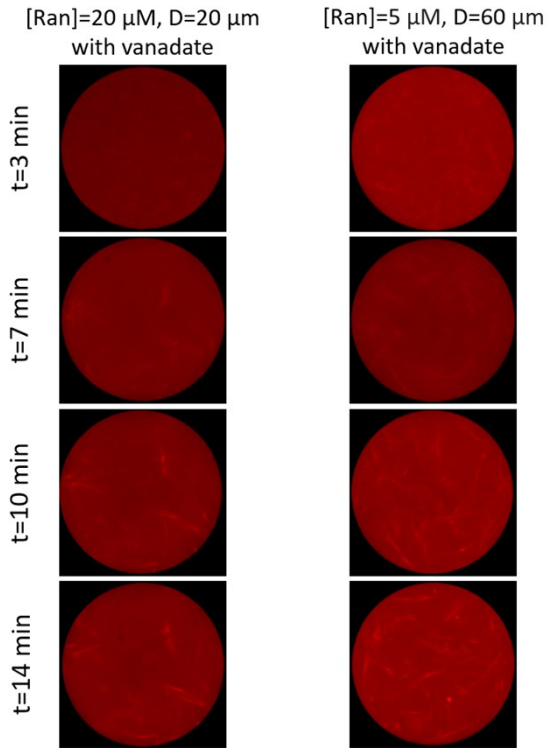


Figure S7. Wide-field images showing the assembly aster structures



**Figure S8. Effect of inhibiting motor activities on the ring and flower assemblies**

We inhibited the motor activities by adding Vanadate. The final vanadate concentration in the droplets was 500 nM.



## Supplementary Information Movies

**Movie S1.** Videos showing ring-shaped MT networks inside droplets with  $D=20\ \mu\text{m}$  and Ran concentrations of  $5\ \mu\text{M}$ ,  $10\ \mu\text{M}$ , and  $20\ \mu\text{M}$ .

**Movie S2.** Videos showing flower-shaped MT networks. The test conditions are  $D=60\ \mu\text{m}$  and  $Ran=5\ \mu\text{M}$ , and  $D=110\ \mu\text{m}$  and  $Ran=5\ \mu\text{M}$ .

**Movie S3.** Videos showing the assembly of MT asters. From left to right, the test conditions are  $D=60\ \mu\text{m}$  and  $Ran=10\ \mu\text{M}$ ,  $D=110\ \mu\text{m}$  and  $Ran=10\ \mu\text{M}$ ,  $D=60\ \mu\text{m}$  and  $Ran=20\ \mu\text{M}$ , and  $D=110\ \mu\text{m}$  and  $Ran=20\ \mu\text{M}$ .

**Movie S4.** Widefield videos showing flower-shaped MT networks. Left:  $[Ran]=5\ \mu\text{M}$  and  $D=60\ \mu\text{m}$ . Right:  $[Ran]=5\ \mu\text{M}$  and  $D=110\ \mu\text{m}$ .

**Movie S5.** Widefield videos showing MT networks with aster architectures. From left to right, the test conditions are  $D=60\ \mu\text{m}$  and  $Ran=10\ \mu\text{M}$ ,  $D=110\ \mu\text{m}$  and  $Ran=10\ \mu\text{M}$ ,  $D=60\ \mu\text{m}$  and  $Ran=20\ \mu\text{M}$ , and  $D=110\ \mu\text{m}$  and  $Ran=20\ \mu\text{M}$ .

**Movie S6.** Videos showing EB1 signals in droplets with  $[Ran]=5\ \mu\text{M}$  and  $[Ran]=10\ \mu\text{M}$ , respectively. The droplets have a size of  $D=60\ \mu\text{m}$ .

**Movie S7.** Effect of inhibiting motor proteins in confined extracts by adding Vanadate. The final concentration of Vanadate in the droplets is  $500\ \text{nM}$ . The droplet size is  $D=110\ \mu\text{m}$ , and the Ran concentration is  $[Ran]=10\ \mu\text{M}$ .